Charge trapping properties at silicon nitride/silicon oxide interface studied by variable-temperature electrostatic force microscopy

S.-D. Tzeng and S. Gwo[a)]
Department of Physics, National Tsing-Hua University, Hsinchu 300, Taiwan, Republic of China

(Received 29 March 2006; accepted 27 April 2006; published online 25 July 2006)

Charge trapping properties of electrons and holes in ultrathin nitride-oxide-silicon (NOS) structures were quantitatively determined by variable-temperature electrostatic force microscopy (EFM). From charge retention characteristics obtained at temperatures between 250 and 370 °C and assuming that the dominant charge decay mechanism is thermal emission followed by oxide tunneling, we find that there are considerable deep trap centers at the nitride-oxide interface. For electron, the interface trap energy and density were determined to be about 1.52 eV and 1.46×10^{12} cm^{-2}, respectively. For hole, these are about 1.01 eV and 1.08×10^{12} cm^{-2}, respectively. In addition, the capture cross section of electron can be extracted to be 4.8×10^{-16} cm^{2}. The qualitative and quantitative determination of charge trapping properties and possible charge decay mechanism reported in this work can be very useful for the characterization of oxide-nitride-silicon based charge storage devices. © *2006 American Institute of Physics*. [DOI: 10.1063/1.2218025]

I. INTRODUCTION

Si_3N_4/SiO_2/silicon [nitride-oxide-silicon (NOS)] electret structure is widely applied to electronic devices such as nonvolatile charge memories. For example, since 1967 by Wegener *et al.*,[1] metal-nitride-oxide-silicon (MNOS) structure and its various derivatives such as metal-oxide-nitride-oxide-silicon (MONOS), silicon-nitride-oxide-silicon (SNOS), and silicon-oxide-nitride-oxide-silicon (SONOS) structures have remained as one of the state-of-the-art techniques for nonvolatile semiconductor memories (NVSMs).[2] ONO-based memories are inexpensive, highly integrated, and can be expanded to store two bits of data per memory cell.[3] The top oxide layer in ONO-based memories, also called the blocking oxide, allows the scaling of nitride layer because it cannot only inhibit gate injection,[4] but also block the charges injected into nitride at the oxide-nitride interface,[5] resulting in a higher trapping efficiency for ultrathin nitride layer. Therefore, the total thickness of the ONO structure (and consequently, the programming voltage) can be reduced. As the thickness of nitride becomes thinner, the charges trapped at top oxide-nitride (ON) and nitride-bottom oxide (NO) interfaces become more considerable relative to charges trapped in the nitride layer. It has been suggested that charges stored at or near the NO interface exhibit both deeper trap energy and longer retention time.[6–8] Hence, the properties of ultrathin ONO memory structures are more likely governed by interface charge traps rather than by the bulk trapping properties of nitride.

Several previous studies have reported that ON or NO interface is responsible for the large amount of captured charges[7–14] and can be explained by the excess silicon at interfaces,[15–17] which can capture both electrons and holes. However, up to now, only a few attempts have been made to quantitatively determine the charge trapping properties at the NO interface. Suzuki and Hayashi have reported that there are abundant trap centers at top oxide-nitride interface with a density of $2.3-2.5\times10^{13}$ cm^{-2} and the capture cross section of $\sim6\times10^{-14}$ cm^{2}.[10] In the work of Ma *et al.*, both ON and NO interface trap densities on the order of 10^{12} cm^{-2} were reported, which depend on the growth conditions of dielectric layers.[18] Kim and Choi reported a deep trap energy of about 1.9 eV near the ON interface.[19] In these works, interface trapping properties of electron were determined. By contrast, only a limited number of reports have discussed the hole trapping properties in nitride or nitride-oxide interface.[17,20,21] Furthermore, the trap energy, density, and capture cross section of trap centers at NO interface have never been simultaneously determined on one set of samples using the same measurement method. Since variations in growth conditions, dielectric stack structures, and measurement techniques can result in a large variation of extracted charge trapping properties, a systematical study of all these trapping properties for both electron and hole on one specific sample set using the same experimental method is highly desirable.

In this work, we employ the technique of variable-temperature electrostatic force microscopy (EFM) to study the trapping properties (trap energy, trap density, capture cross section, etc.) of elementary charges (both electron and hole) in ultrathin NOS structures. The contact potential difference (CPD) induced by electrons or holes trapped in the electret structures is directly measured by EFM under high-vacuum conditions. Thus, the transistor structure such as that used in ONO-based memory is not needed for determining charge trapping properties. Moreover, the vacuum gap between electret sample and the EFM tip can inhibit charges escaping or injection. As a result, the top blocking oxide layer conventionally used to separate the nitride layer from the conducting gate is also not necessary. These advantages allow us to study the interface trapping properties by using a simple, as-grown NOS structure, which has only one nitride-

[a)]Electronic mail: gwo@phys.nthu.edu.tw

oxide interface. And, it is easier for data analysis in comparison to the more complicate ONO-based device structures.

Although charges could also be trapped in oxide or oxide-silicon interface,[22] their retention times are much shorter than that of charges trapped in nitride or at nitride-oxide interface. Kang *et al.*[23] reported a retention time on the order of 120 s using scanning capacitance microscopy. Buh *et al.*[24] have also studied the decay of trapped charge in an oxide-silicon structure using EFM. They demonstrated that both negative and positive charges are trapped with the density on the order of 10^{10} cm^{-2} and the retention time on the order of 10^3 s. The same order of magnitude of retention time was also reported in the work of Paulsen *et al.*[25] using the charge-pumping technique. All the retention times reported in these works were measured at room temperature. Since the data acquired in our work was measured at temperatures between 250 and 370 °C, the oxide charges would detrap rapidly with the retention time much shorter than 10^3 s. Consequently, we assume the trapped oxide charges are not significant in our variable-temperature EFM measurements. Furthermore, in our technique, the measured CPD represents the contact potential difference between charged and uncharged surface regions. Therefore, all intrinsic charges uniformly distributed in the sample, which are irrelevant to the injected charges, can be treated as background and eliminated in the CPD measurements.

II. SAMPLE PREPARATION AND EFM MEASUREMENTS

The silicon oxide and silicon nitride thin layers in our NOS samples were formed by thermal oxidation (in dry O_2 at 900 °C) and low-pressure chemical vapor deposition (in a mixture of $SiCl_2H_2$ and NH_3 at 750 °C), respectively, on *p*-type Si(001) wafers with a resistivity of about 10 Ω cm. The layer thickness of oxide (d_{ox}) was 22 Å for all samples. The layer thickness of nitride (d_n) was 30 Å for sample NOS(30/22) and 61 Å for sample NOS(61/22), respectively. These thicknesses were measured by ellipsometry.

The charge trapping properties in NOS samples were quantitatively determined by an environment-controlled, variable-temperature scanning probe microscopy system (Seiko Instruments, SPA-300HV). Both detection and injection of charges were performed under high-vacuum conditions (10^{-6}–10^{-7} Torr), which allow higher charge detection sensitivity and prevent the local charging process from the effects of probe-induced anodic oxidation.[26,27] Probes used in this work were PtIr-coated Si probes with a typical tip radius of about 20 nm and were electrically grounded. When the probe was not used for charge detection or injection (such as during the thermal detrapping process of stored charges), it was lifted away from the sample surface. During measurements, the probe was operated under the intermittent contact mode with tip oscillation amplitude of ~100 nm and at oscillation frequency f_0 of ~60 kHz (slightly lower than its resonance frequency). Both ac and dc voltages $[V_{ac}\sin(2\pi f_1 t)+V_{dc}]$ were applied to the silicon substrate, where the dc voltage V_{dc} could be adjusted to nullify the output signal of lock-in amplifier (i.e., the EFM signal) on the surface [this operation mode is also called Kelvin probe force microscopy (KPFM)]. The EFM signal measured the electrostatic force at the modulation frequency ($f_1 \approx 65$ kHz). Figure 1 shows the schematic drawing of the EFM system. By using the dual-modulation scheme at two noninterfering modulation frequencies (f_0 and f_1), AFM surface topography and EFM charge image can be simultaneously obtained.

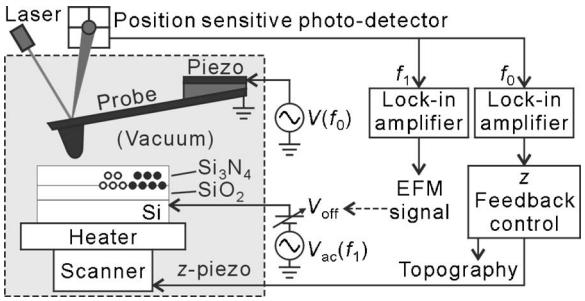

FIG. 1. Schematic drawing of the environment-controlled EFM system. The surrounding pressure of the sample is typically 10^{-6}–10^{-7} Torr. The temperature of heater is controlled by a thermocontroller. Moreover, the temperature of sample is calibrated by a thermocouple.

While injecting charges, the probe was operated under the contact mode in high vacuum and at room temperature. By applying a charge injection bias V_{inj} at silicon substrate, charges can tunnel from the tip and then are trapped in the nitride layer or at the NO interface. In this process, the bottom oxide plays the role of the blocking oxide, which not only efficiently blocks charges crossing at the NO interface, but also prevents charges injection from the silicon substrate. Figure 2(a) shows the EFM charge images of charge lines and dots on the NOS(30/22) sample. The charge lines were created at room temperature with $V_{inj}=-7$ V/+6 V and tip scan speed of ~1 mm/s. The charge dots were created with $V_{inj}=\pm 10$ V square wave at frequency of 10 kHz and tip scan speed of ~1.4 mm/s. These results indicate that both electrons and holes can be injected from the conducting tip into the NOS(30/22) sample with voltage pulses of ~10 μs and $V_{inj}<10$ V.

The charges trapped in the nitride layer or at the NO interface can escape from their trap sites at elevated temperatures. The determination of possible escape pathways is important for understanding the charge decay mechanism. Figure 2(b) displays the EFM images of charge lines and dots in the same areas as Fig. 2(a) after heating at 200 °C for ~1300 and ~1150 min, respectively. And, Fig. 2(c) shows the averaged line profiles of EFM signals deduced from charge images shown in Figs. 2(a) and 2(b). The decrease of EFM signal after prolong sample heating indicates that some trapped charges have escaped from the trapping sites. However, the linewidths of the EFM profiles do not broaden significantly after heating. This experimental observation can be explained by using the charge decay mechanism that the escaped charges tunnel into the silicon substrate before their possible lateral diffusion. Consequently, in this work, we assume that the dominant decay mechanism is thermal emission followed by oxide tunneling process.

The EFM signal, as shown in Fig. 2, is not a simple

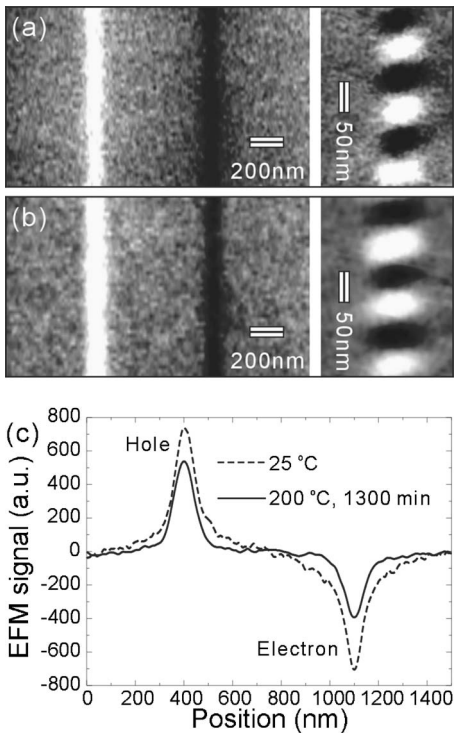

FIG. 2. Relaxation of charges in the NOS(30/22) sample heated at 200 °C in vacuum. (a) EFM images of charge lines and dots, which were created and measured at about 25 °C. The charge lines were written with V_{inj} =−7 V/+6 V and tip scan speed≈1 mm/s. The charge dots were written with V_{inj}=±10 V (square wave) with frequency of 10 kHz and tip scan speed of ~1.4 mm/s. (b) EFM images of the charge lines and dots after heating at 200 °C for ~1300 and ~1150 min, respectively. (c) The averaged line profile of charge lines obtained from (a) and (b).

function of the density of charges in NOS, but proportional to the product of $\partial C/\partial d$ and $(\mathrm{CPD}+V_{off}-V_{off}^0)V_{ac}$.[28,29] The offset voltage on the NOS surface without injected charges, V_{off}^0 (the contact potential difference between the tip and the Si surface beneath the uncharged NO stack), is typically about −700 mV at room temperature. On the charged NOS surface, the offset voltage (V_{off}) is V_{off}^0–CPD for nullified EFM signal, where CPD is positive (negative) on positively (negatively) charged surface. Although $\partial C/\partial d$ depends on the capacitance C between the tip and the sample (a function of tip-sample geometry) and the tip-to-sample distance d, the value of $\partial C/\partial d$ is irrelevant when EFM signal is nullified (i.e., $\mathrm{CPD}+V_{off}-V_{off}^0=0$). Therefore, the shape and vertical position of tip do not have any significant influence on the CPD measurement. Although the modulation amplitude V_{ac} typically equals to 0.5 V in our measurements, the CPD value does not change significantly with V_{ac} in the range of 0.1–1.0 V. This indicates that the space-charge density in silicon can be considered as a quasistatic distribution.

The CPD measured on NOS can be related to the spatial distribution of charges, which in principle can be calculated by solving the Poisson equation.[30] To quantitatively determine the charge trapping properties, charges were injected into 2×2 μm^2 squares and the CPD values were measured on the center of charged areas to avoid the boundary effects. Figures 3(a) and 3(b) show the CPD images of negatively and positively charged areas on NOS(30/22) with V_{inj}=+8 and −8 V, respectively. These images were measured at

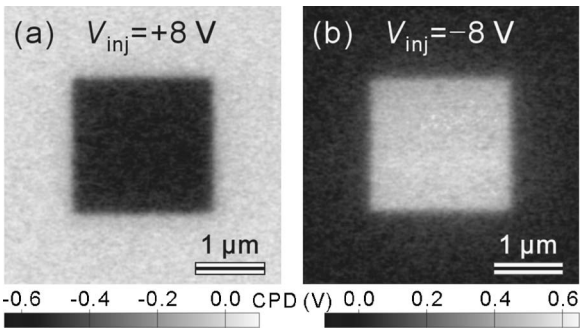

FIG. 3. CPD images of negatively (a) and positively (b) charged areas on NOS(30/22) with V_{inj}=+8 and −8 V, respectively. Charges in these 2×2 μm^2 squares were injected at room temperature by 256 scan lines at 4 μm/s tip scan speed and measured at 250 °C after baked at this temperature for about 16 h.

250 °C after the sample was baked at this temperature for about 16 h. The CPD values on the centers of negatively and positively charged areas are about −530 and +500 mV, respectively. The uncertainty of CPD measurement is typically only about 30 mV. The good lateral uniformity of CPD implies a uniform distribution of trapped charges in the lateral directions. Therefore, the space-charge density in silicon substrate $\rho_{si}(x,y,z)$ could be written as $\rho_{si}(z)$ (unit: traps/cm^3), where z is the axis perpendicular to the surface. By using one-dimensional Poisson equation, the static surface charge density on silicon (unit: traps/cm^2) could be written as[31]

$$\sigma_{si}(\psi_{si},T)=\int \rho_{si}(z)dz = \mp\frac{\sqrt{2}\varepsilon_{si}}{\beta L_D}\left\{[\exp(-\beta\psi_{si})+\beta\psi_{si}-1]+\frac{n_{po}}{p_{po}}[\exp(\beta\psi_{si})-\beta\psi_{si}-1]\right\}^{1/2}, \quad (1)$$

where ψ_{si} is the electrical potential at silicon surface, T is the absolute temperature of sample, ε_{si} is the permittivity of silicon, n_{po} and p_{po} are the equilibrium densities of electrons and holes in the bulk of p-type silicon, $\beta\equiv q/k_BT$ (q is the electronic charge and k_B is the Boltzmann's constant), and $L_D\equiv\sqrt{\varepsilon_{si}/qp_{po}\beta}$ is the extrinsic Debye length for hole. In Eq. (1), the positive sign is used for $\psi_{si}<0$ and the negative sign is for $\psi_{si}>0$. Figures 4(a) and 4(b) show schematic band diagrams of the NOS structure with $\psi_{si}>0$ and $\psi_{si}<0$, respectively. While measuring CPD, the static surface charge density (σ_m) on the tip is zero since the electrostatic force is nullified by adjusting V_{off}. This is equivalent to that the static electric field in the space between the tip and the sample surface is zero. Therefore, the total static charge density in NOS is also zero: $\int\rho_n(z)dz+\sigma_i+\int\rho_{si}(z)dz=0$, where $\rho_n(z)$ (unit: traps/cm^3) is the trapped charge density in nitride film and σ_i (unit: traps/cm^2) is the trapped charge density at NO interface. If we assume $\rho_n(z)$ is uniform, i.e., $\rho_n(z)=\rho_n$, using the Gauss' law, we can obtain

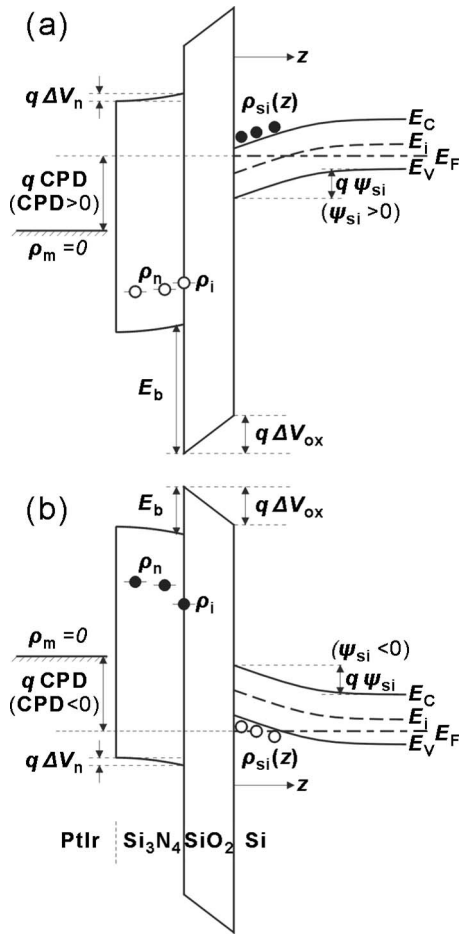

FIG. 4. Schematic band diagrams of the NOS structure with $\psi_{si}>0$ (a) and $\psi_{si}<0$ (b), respectively.

$$\mathrm{CPD} = \psi_{si} + \Delta V_n + \Delta V_{ox} = \psi_{si} + \rho_n d_n\left(\frac{d_n}{2\varepsilon_n} + \frac{d_{ox}}{\varepsilon_{ox}}\right) + \sigma_i \frac{d_{ox}}{\varepsilon_{ox}}, \quad (2)$$

where ε_{ox} and ε_n are the permittivities of silicon oxide and silicon nitride, respectively. Thus, the ψ_{si} could be determined from

$$\sigma_{si}(\psi_{si}, T) = -\sigma_t = -\sigma_i - \rho_n d_n, \quad (3)$$

where σ_t is the total trapped charge density (unit: traps/cm^2). If we know the value of ρ_n and σ_i, we can obtain the relationship between CPD and σ_t from Eqs. (1)–(3). Figure 5 shows the calculated results of CPD as a function of σ_t on the NOS sample with different parameters (d_n, σ_i, ρ_n, and T), which can be used for the conversion of measured CPD values to trap charge densities.

III. QUANTITATIVE MODELING OF CHARGE RETENTION

To determine the trap energies of charges trapped in nitride or at NO interface, we studied their retention behavior at elevated temperatures. Figure 6 shows some possible charge decay processes in an ultrathin NOS structure:

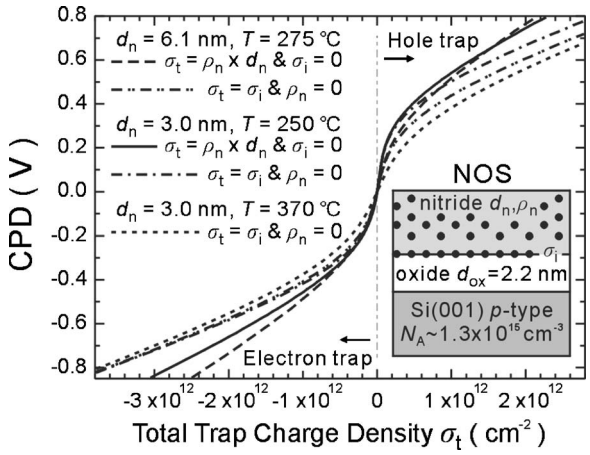

FIG. 5. Calculated results of CPD as a function of σ_t on the NOS structures with different d_n, σ_i, ρ_n, and T. A positive (negative) σ_t represent holes (electrons) trapped at the NO interface and in the nitride layer. An impurity concentration of p-type silicon $N_A = 1.3\times10^{15}$ cm^{-3} was used for the calculation.

(1) Direct tunneling of electrons (holes) through the oxide from the NO interface trap centers into the silicon conduction (valence) band. The tunneling probability is denoted as e_{tb}.
(2) Thermal excitation of trapped electrons (holes) from the trap centers in nitride or at NO interface to the nitride conduction (valence) band. The thermal emission rate is denoted as e_{th} when we employ the Shockley-Read-Hall (SRH) model[32,33] and is denoted as e_{esc} when we apply the simple quantum mechanical model suggested by Aozasa *et al.*[34]
(3) Direct tunneling of electrons (holes) through the oxide from the nitride conduction (valence) band into the silicon conduction (valence) band. The probability of this oxide tunneling is denoted as e_{bb}.

Although direct tunneling of electrons (holes) from the NO interface traps into the oxide-silicon interface trap state

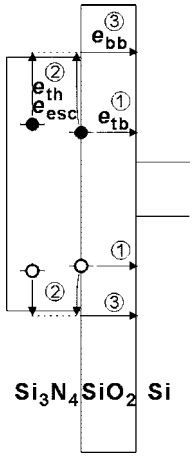

FIG. 6. Some possible charge decay processes in the ultrathin NOS structure: (1) Direct tunneling of trapped electron (hole) from the NO interface trap into the silicon conduction (valence) band with tunneling probability e_{tb}. (2) Thermal excitation of trapped electron (hole) from the trap center in nitride or at NO interface to the nitride conduction (valence) band with thermal emission rate e_{th} or e_{esc}, depending on the model adopted. (3) Direct tunneling of electron (hole) from the nitride conduction (valence) band into the silicon conduction (valence) band with tunneling probability e_{bb}.

is also possible,[6] its tunneling probability e_{tt} is much smaller than e_{tb}. Therefore, this trap-to-trap charge decay processes are ignored here.

At high temperatures (typically above 150 °C), the thermal excitation dominates the charge decay process.[20] In this work, retention behaviors were studied at temperatures between 250 and 370 °C. Therefore, we assume that the thermal emission followed by oxide tunneling process is the main decay process, and the retention time τ of trapped charges can be written as

$$\tau = \frac{1}{e_{\text{th}} e_{\text{bb}}} \text{ or } \tau = \frac{1}{e_{\text{esc}} e_{\text{bb}}}. \tag{4}$$

If we assume that the oxide forms a rectangular barrier for charge tunneling and the influence of image forces can be neglected, e_{bb} can be given by

$$e_{\text{bb}} = \exp(-2 d_{\text{ox}} \sqrt{2 m_{\text{ox}}^{*} E_b}/\hbar), \tag{5}$$

where E_b is the energy barrier for tunneling (conduction or valence band discontinuity between nitride and oxide), m_{ox}^{*} is the effective mass of elementary charge in silicon oxide, $\hbar$ is the reduced Planck constant. The thickness of oxide (d_{ox}) is 22 Å in this work. For electron, $e_{\text{bb}} = 3.18 \times 10^{-7}$ if $E_b = 1.05$ eV (Ref. 35) and $m_{\text{ox}}^{*} = 0.42 m_0$ (Ref. 36) are used. For hole, $e_{\text{bb}} = 2.34 \times 10^{-10}$ if $E_b = 2.85$ eV (Ref. 25) and $m_{\text{ox}}^{*} = 0.34 m_0$ are used.[37] Here m_0 is the free electron mass.

Using the approach originated by Shockley, Read, and Hall,[32,33] the thermal emission rate e_{th} could be written as[38]

$$e_{\text{th}} = 2\sigma_c \left(\frac{3 k_{\text{B}} T}{m_n^{*}} \right)^{1/2} \left(\frac{2\pi m_n^{*} k_{\text{B}} T}{h^2} \right)^{3/2} \exp(-E_t/k_{\text{B}} T) \tag{6}$$

or

$$e_{\text{th}} = \alpha T^2 \exp(-E_t/k_{\text{B}} T) \tag{7}$$

where σ_c is the capture cross section, m_n^{*} is the effective mass in nitride, h is the Planck constant, E_t is the trap energy, and α is the combination of temperature independent constants in Eq. (6). From Eqs. (4) and (7), the retention time τ at temperature T can be given by

$$\tau = \frac{1}{\alpha e_{\text{bb}} T^2} \exp(E_t/k_{\text{B}} T). \tag{8}$$

This implies that charges with larger trap energies also show longer retention times at a given temperature. Besides, Eq. (8) can be further written as

$$\log(\tau T^2) = -\log(\alpha e_{\text{bb}}) + \frac{E_t}{2.3 k_{\text{B}}} \frac{1}{T}. \tag{9}$$

Therefore, if retention times at different temperatures are determined, the trap energy E_t and the temperature independent constants α can also be determined from the linear relationship between $\log(\tau T^2)$ and $1/T$. Since the retention time τ depends on the trap energy E_t, i.e., $\tau = \tau(E_t)$, the retention behavior of charges trapped with trap energy E_t can be written as

$$\rho_n(E_t, t) = \rho_{n0}(E_t) \exp[-t/\tau(E_t)] \tag{10}$$

for charges trapped in the nitride layer, and

$$\sigma_i(E_t, t) = \sigma_{i0}(E_t) \exp[-t/\tau(E_t)] \tag{11}$$

for charges trapped at the NO interface. Here, $\rho_{n0}(E_t)$ (unit: traps $\text{cm}^{-3}\,\text{eV}^{-1}$) and $\sigma_{i0}(E_t)$ (unit: traps $\text{cm}^{-2}\,\text{eV}^{-1}$) are the initial trapped charge density at trap energy E_t in the nitride layer and at the NO interface, respectively. Then, the total trapped charge density of all trap energies in the bulk nitride layer and at the NO interface can be written as

$$\rho_n(t) = \int_{E_{gn}} \rho_n(E_t, t) dE_t, \tag{12}$$

and

$$\sigma_i(t) = \int_{E_{gn}} \sigma_i(E_t, t) dE_t, \tag{13}$$

respectively. Here the subscript E_{gn} indicates the integration is performed with the entire nitride band gap. From Eq. (3), the total trapped charge density can be written as

$$\sigma_t(t) = \rho_n(t) d_n + \sigma_i(t) = \int_{E_{gn}} \sigma_{t0}(E_t) \exp[-t/\tau(E_t)] dE_t, \tag{14}$$

where $\sigma_{t0}(E_t) = \rho_{n0}(E_t) d_n + \sigma_{i0}(E_t)$ is the initial total trapped charge density at trap energy E_t.

In the simple quantum mechanical model, the thermal emission rate e_{esc} is given by

$$e_{\text{esc}} = A_{\text{esc}} \exp(-E_t/k_{\text{B}} T), \tag{15}$$

where A_{esc} is the attempt-to-escape frequency. From simple quantum mechanical model, $A_{\text{esc}} \approx E_t/h$ is a temperature independent constant. From Eqs. (4) and (15), the retention time τ at temperature T is given by

$$\tau = \frac{1}{A_{\text{esc}} e_{\text{bb}}} \exp(E_t/k_{\text{B}} T). \tag{16}$$

In contrast to Eq. (9), the relationship between trap energy E_t and attempt-to-escape frequency A_{esc} can be determined from

$$\log(\tau) = -\log(A_{\text{esc}} e_{\text{bb}}) + \frac{E_t}{2.3 k_{\text{B}}} \frac{1}{T}. \tag{17}$$

Since e_{th}, as described in Eq. (7), is proportional to T^2, e_{esc} is larger than e_{th} at low temperatures. Although the simple quantum mechanical model is typically used for temperatures below 150 °C, the feasibility of this model is also verified by comparing the extracted value of A_{esc} with αT^2, as described below in the discussion section.

IV. EXPERIMENTAL RESULTS

Figure 7(a) shows the variation of CPD with time t measured on NOS(30/22) at 250 °C. To obtain the value of retention time τ, the relationship between total trapped charge density σ_t and time t is required. From Eqs. (1)–(3), we can convert the value of CPD to σ_t when the values of ρ_n and σ_i are known. Since ρ_n and σ_i have not been determined yet, we cannot directly convert the CPD value to σ_t. However, we can assume two extreme charge distributions: (I) $\sigma_t = \sigma_i$ and $\rho_n = 0$; (II) $\sigma_t = \rho_n d_n$ and $\sigma_i = 0$. By using the correlative

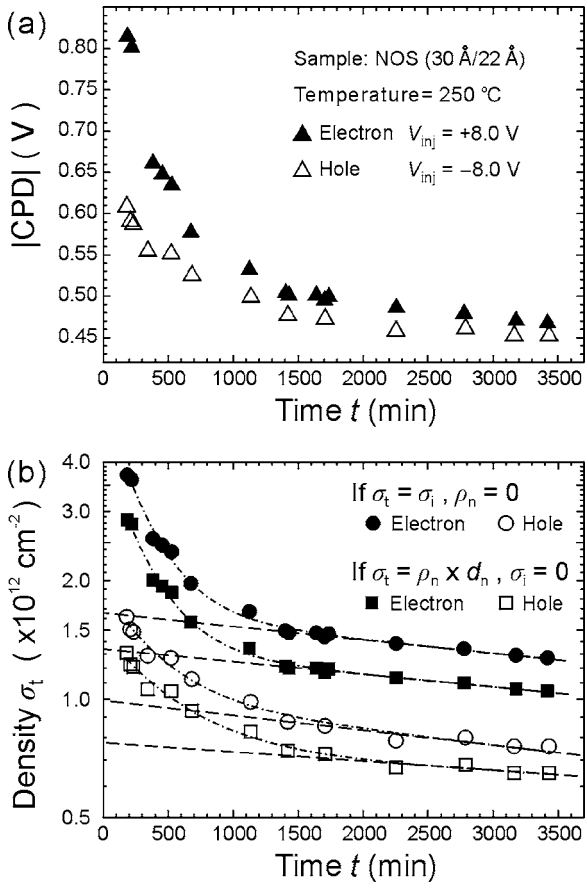

FIG. 7. (a) The variation of CPD value with time t on NOS(30/22) at 250 °C. (b) The $\log(\sigma_t)$-t plot with two corresponding possible values of σ_t, which are converted from the CPD values by assuming two extreme charge distributions: (I) $\sigma_t=\sigma_i$ and $\rho_n=0$; (II) $\sigma_t=\rho_n d_n$ and $\sigma_i=0$.

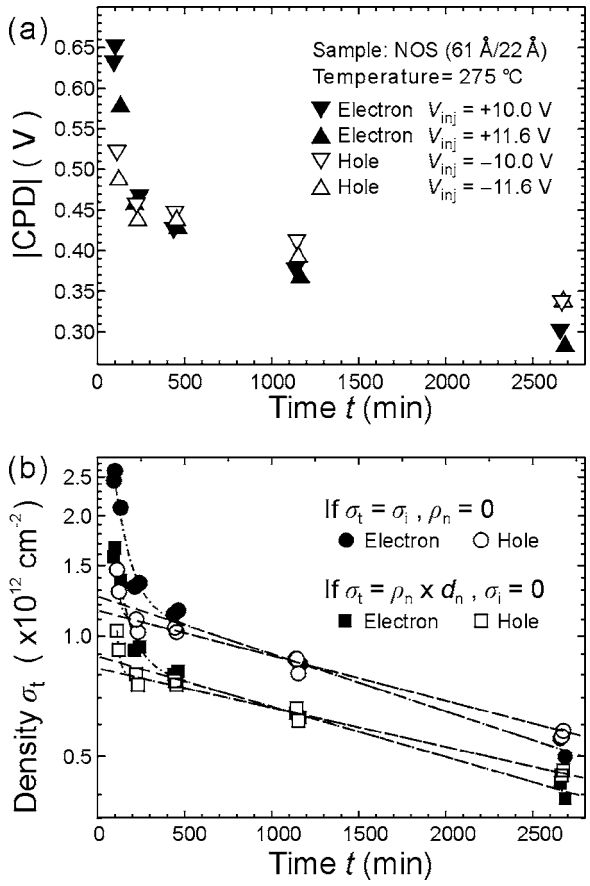

FIG. 8. (a) The variation of CPD value with time t on NOS(61/22) at 275 °C. (b) The $\log(\sigma_t)$-t plot with two corresponding possible values of σ_t, which are converted from the CPD values by assuming two extreme charge distributions: (I) $\sigma_t=\sigma_i$ and $\rho_n=0$; (II) $\sigma_t=\rho_n d_n$ and $\sigma_i=0$.

curves shown in Fig. 5 for converting CPD to σ_t, we obtain two corresponding values of $\sigma_t(t)$ with respect to the two extreme distributions, as shown in Fig. 7(b). Since the realistic trapped charge distribution lies in between these two extreme charge distributions, the real value of σ_t at time t also lies in between these two values of $\sigma_t(t)$. In Fig. 7(b), both electrons and holes, with respect to these two distributions, show the similar retention behavior: σ_t decreases quickly in the first 30 h of sample heating and then decay exponentially; i.e., it follows a linear relationship in the $\log(\sigma_t)$-t plot. From Eqs. (8), (10), and (11), this exponential decay implies a single-valued τ and also a constant deep trap energy E_{td}. Besides, the relatively long τ also means that charges remained trapped at $t>1800$ min with the deep trap energy of E_{td}. If the trap centers related to E_{td} are distributed at NO interface, i.e, $\sigma_{t0}(E_{td})=\sigma_{i0}(E_{td})$, the initial charge density $\sigma_{t0}(E_{td})$ is $1.66\pm0.21\times10^{12}$ cm^{-2} for electron and is $1.00\pm0.16\times10^{12}$ cm^{-2} for hole. If these deep trap centers are uniformly distributed in nitride, i.e., $\sigma_{t0}(E_{td})=\rho_{n0}(E_{td})d_n$, $\sigma_{t0}(E_{td})$ is $1.33\pm0.21\times10^{12}$ cm^{-2} for electron and is $0.75\pm0.15\times10^{12}$ cm^{-2} for hole.

To locate the exact spatial locations of these deep trap centers, we performed a control experiment on NOS(61/22) at 275 °C. Since oxide and nitride films on all samples were grown under identical conditions $\rho_{n0}(E_{td})$ and $\sigma_{i0}(E_{td})$ between different NOS samples should be the same when all trap sites in NOS are filled. Figure 8(a) shows the CPD changed with time t on NOS(61/22), where charges were initially injected by four different V_{inj} (±11.6 and ±10 V). In Fig. 8(a), electrons (holes) injected with $V_{inj}=+11.6$ V (−11.6 V) have about the same CPD as injected with $V_{inj}=+10$ V (−10 V), implying that all the trap sites in NOS(61/22) had been filled up with $V_{inj}=\pm11.6$ V, which corresponds to an electrical field of about 11.7 MV/cm in the nitride film. The same electric field also occurred on NOS(30/22) with $V_{inj}=\pm8$ V. Accordingly, it is reasonable to assume that all trap sites are initially filled on both samples. Therefore, if the deep trap sites are distributed at NO interface, their initial charge density $\sigma_{i0}(E_{td})$ on NOS(61/22) remains the same as NOS(30/22). However, if they are uniformly distributed in nitride, their initial charge density $\rho_{n0}(E_{td})d_n$ on NOS(61/22) will approximately double since d_n increases from 30 to 61 Å. Figure 8(b) shows the $\log(\sigma_t)-t$ plot with two possible values of σ_t, which are converted from CPD by using the correlative curves shown in Fig. 5. In the case of all deep traps distributed at the NO interface, the initial charge density is $1.26\pm0.20\times10^{12}$ cm^{-2} for electron and $1.16\pm0.16\times10^{12}$ cm^{-2} for hole. In the case of all deep traps uniformly distributed in nitride, the initial charge density is $0.89\pm0.20\times10^{12}$ cm^{-2} for electron and $0.83\pm0.16\times10^{12}$ cm^{-2} for hole. After comparing all possible $\rho_{n0}(E_{td})$

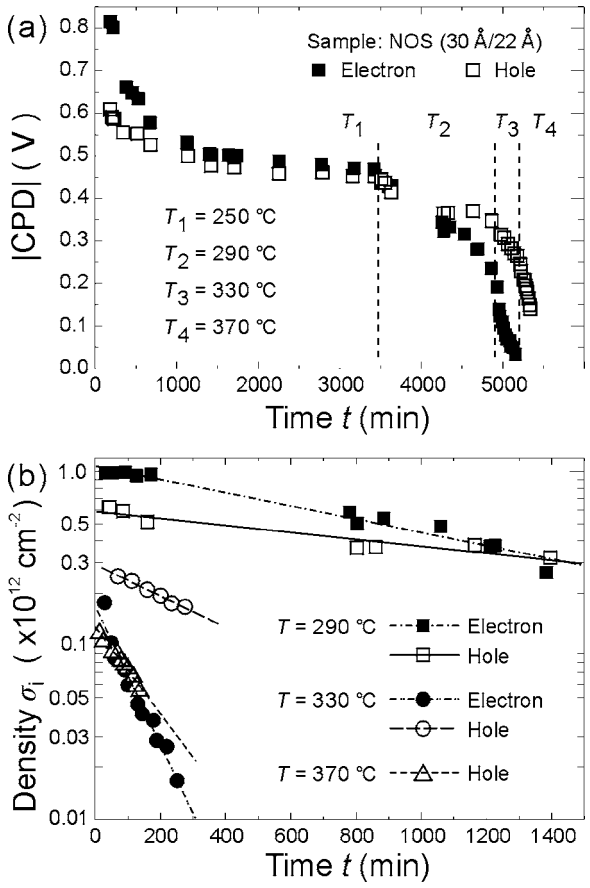

FIG. 9. (a) The variation of CPD value with time t on NOS(30/22) at 250, 290, 330, and 370 °C. (b) Their corresponding $\log(\sigma_i)$-t plots with time, appropriately adjusted at each temperature.

and $\sigma_{i0}(E_{td})$ shown in Figs. 7(b) and 8(b), we deduce that these deep trap centers are distributed at the NO interface. Besides, their initial charge density $\sigma_{i0}(E_{td})$ is $1.46\pm0.30\times10^{12}$ cm^{-2} for electron and $1.08\pm0.23\times10^{12}$ cm^{-2} for hole.

Finally, to determine E_{td} of these deep trap centers distributed at the NO interface, we studied their retention behavior at different temperatures. Figure 9(a) shows the CPD variation with time t on NOS(30/22) at 250, 290, 330, and 370 °C. The data acquired at 250 °C are identical to the data shown in Fig. 5(a), where only charges at the NO interface remained at the end. Therefore, the subsequent data acquired at higher temperatures also represent the retention behavior of charges trapped at the NO interface. Figure 9(b) shows the corresponding $(\log\sigma_i)-t$ plot with the time appropriately adjusted at each temperature. The linear relationship shown in Fig. 9(b) represents a well-defined retention time τ at each temperature T. Figure 10 shows the relationship between τT^2 and $1/T$, where τ of interface charges at different temperatures come from the fitting results in Figs. 7(b) and 9(b). The linear relationship shown in Fig. 10 also indicates single, well-defined trap energy. These results imply that these charges are trapped at the same type of trap centers. From Eq. (9), we obtain the trap energy of these interface trap centers is 1.52 ± 0.10 eV for electron and 0.91 ± 0.06 eV for hole. Besides, the value of αe_{bb} is about 2.20×10^3 K^{-2} for electron, resulting in the temperature independent constants

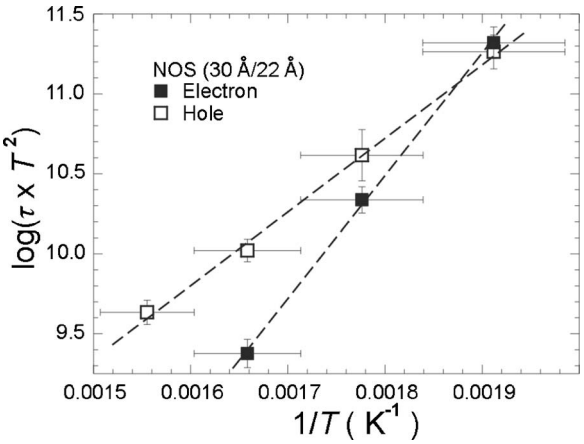

FIG. 10. The relationship between τT^2 (unit: s K^2) and $1/T$ of electrons and holes trapped at the NO interface.

$\alpha=6.91\times10^9$ K^{-2}, which is of the same order of magnitude as the result of Kim *et al.*[39] ($\sim2.2\times10^9$ K^{-2}). For hole, αe_{bb} is about 3.60×10^{-3} K^{-2}, resulting in $\alpha=1.54\times10^7$ K^{-2}.

V. DISCUSSION

The prior trap energies were extracted by assuming that thermal emission followed by oxide tunneling is the dominant decay mechanism. Two types of thermal emission rate, e_{th} and e_{esc}, based on two different thermal models are employed in our work. The valid condition of the SRH model is $e_{th}>e_{esc}$. From Eqs. (7) and (15), this condition becomes $\alpha T^2>A_{esc}\approx E_t/h$. For electron traps, it is valid when temperature $T>230$ K. Since T in our experiments is 523–643 K, SRH model remains valid. And, the determined electron trap energy is ~1.52 eV. By contrast, the valid condition of SRH model for hole traps is $T>3780$ K. Therefore, the thermal emission rate for hole should be taken from the simple quantum mechanical model. Figure 11 shows the relationship between τ and $1/T$. Using Eq. (17), the interface trap energy for hole is determined to be 1.01 ± 0.03 eV. Besides, the value $A_{esc}e_{bb}\approx9.06\times10^3$ Hz is also extracted, resulting in the attempt-to-escape frequency $A_{esc}\approx3.86\times10^{13}$ Hz. Although $E_t/h\approx2.45\times10^{14}$ Hz is about six times the value of this extracted A_{esc}, this difference may

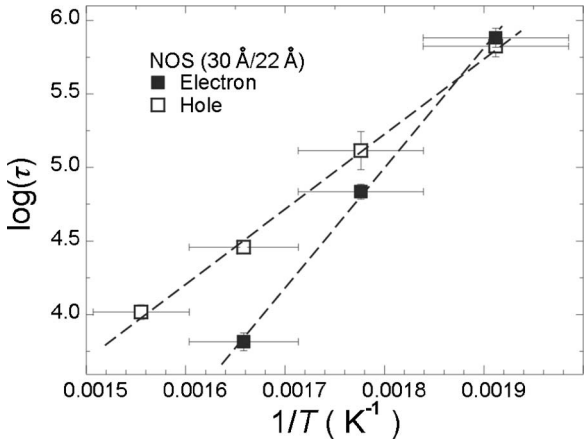

FIG. 11. The relationship between τ (unit: s) and $1/T$ of electrons and holes trapped at the NO interface.

simply come from the error of e_{bb}. Because the value of e_{bb} exponentially depends on d_{ox} and $\sqrt{m^*_{ox}E_b}$, small uncertainties of d_{ox}, m^*_{ox}, and E_b may result in a considerable error of e_{bb}. Therefore, it is possible that $A_{esc}=E_t/h$ is also valid for hole traps, as the case of electron traps suggested by Aozasa *et al.*[34]

Although different types of thermal emission rate between electron and hole is suggested in this work, the difference in extracted values of trap energy between these two models is only about 0.1 eV. By using the simple quantum mechanical model, extracted interface trap energy is 1.62 ± 0.04 eV for electron and 1.01 ± 0.03 eV for hole. By using the SRH model, it is 1.52 ± 0.10 eV for electron and 0.91 ± 0.06 eV for hole. As a result, the electron interface trap energy is much larger than the hole interface trap energy, no matter which model is used.

Since the interface trap centers have deeper trap energies, they are more suitable for charge storage because of their extremely long retention time. For example, if all electrons are trapped at the NO interface (with $d_{ox}=22$ Å), the retention time, predicted from Fig. 10, could be about 120 years at 150 °C. As a result, using NOS or ONOS with ultrathin nitride layer can effectively reduce the number of charges with smaller trap energies, resulting in an increase of the retention time of memory cell. Therefore, the deep trap centers at NO interface may explain the large activation energy obtained in the studies of ONOS flash memories.[3,19,40]

Since the value α for electron trap has been determined, the capture cross section σ_c can be extracted by using Eqs. (6) and (7). Taking $m^*_n=0.4m_0$,[41] we obtain $\sigma_c\sim4.8\times10^{-16}$ cm^2, which corresponds to an effective radius $r_0\approx1.23$ Å. In comparison with the covalent radius of a silicon, 1.17 Å, it suggests that Si–Si defects may be responsible for the deep traps for electrons.[42] From the Mott's model,[43] an electron (or hole) trapped at the neutral Si–Si bond can induce a Coulomb force to its surrounding atoms and results in their displacements. The displacements of ions can then form a potential to the trapped electron. By introducing an effective radius $r_0=1.23$ Å, we obtain the trap energy from Mott's formula: $E_t\approx q^2/4\pi\varepsilon_n r_0\approx1.67$ eV, which agrees well with our result: $E_{td}\approx1.52$ eV. Gritsenko *et al.* have also reported a similar value of trap energy.[44] However, the capture cross section obtained in their results is on the order of 10^{-13} cm^2. Such a large capture cross section was also detected in many studies on nitride or nitride-oxide interface.[11,45–47] We believe that the dissimilarity in the capture cross section might come from the different nature between thermally assisted discharge and electric field assisted discharge. Gritsenko suggested that large capture cross section in the model of Si–Si defect may be due to its polarization under the electric field.[42] In this case, charge may escape from one trap site assisted by the electric field and then be captured by another trap site, which shows long-range dipole potential induced by the electric field. Thus, large capture cross section is acquired by using the current-voltage characteristics or the redistribution of charges after applying a voltage.

The Si–Si defect has been thought as an amphoteric trap center, i.e., both electron and hole can be trapped in a Si–Si defect, resulting in the same trap density for electron and hole. In our results, the densities of deep trap centers at NO interface are estimated to be $1.46\pm0.30\times10^{12}$ cm^{-2} for electron and $1.08\pm0.23\times10^{12}$ cm^{-2} for hole. Moreover, electron and hole trap energies are quite dissimilar (1.52 ± 0.10 vs 1.01 ± 0.03 eV). Although a different hole trap energy was also reported in the Si–Si defect model and might be explained by the asymmetric relaxation of the silicon atoms while the Si–Si bond with captured hole,[17] the large difference in trap densities indicates that the hole trap might have a different origin. Since many properties of Si–Si defects or other possible candidates of deep trap centers have not been well confirmed yet, our results could be useful for ascertaining the origin of trap centers in NOS, at least for the interface electron traps.

VI. SUMMARY

We have studied the charge trapping properties for both electron and hole at high temperatures by using EFM. We find that there are considerable trap centers for both electron and hole with deep trap energies in the NOS structure. We have determined that these deep trap centers are located at the nitride-oxide interface with a density of $1.46\pm0.30\times10^{12}$ cm^{-2} for electron and $1.08\pm0.23\times10^{12}$ cm^{-2} for hole. By assuming thermal emission followed by oxide tunneling process as the dominant charge decay mechanism, the trap energies of these deep trap centers are estimated to be 1.52 ± 0.10 eV for electron and 1.01 ± 0.03 eV for hole. Furthermore, we find that the thermal emission rate of the deep traps can be described as $e_{th}=\alpha T^2\exp(-E_t/k_BT)$ for electron, and $e_{esc}=A_{esc}\exp(-E_t/k_BT)$ for hole. From the temperature independent constant α of electron, we obtained the electron capture cross section $\sigma_c\approx4.8\times10^{-16}$ cm^2. These results support the Si–Si defect (excess silicon) model for interface electron traps. The determination of trapping properties and possible decay mechanism for both electron and hole can be beneficial for the detailed characterization of ONO-based memory cells.

ACKNOWLEDGMENTS

This work was supported by the National Nanoscience and Nanotechnology Project (NSC 94-2120-M-007-002). The authors thank J.-L. Hsieh of Nano Device Laboratory (NDL) for the supply of NOS samples.

[1] H. A. R. Wegener, A. J. Lincoln, H. C. Pao, M. R. O'Connel, and R. E. Oleksiak, Tech. Dig.IEEE IEDM **70** (1967).
[2] *Nonvolatile Semiconductor Memory Technology: A Comprehensive Guide to Understanding and Using NVSM Devices*, edited by W. D. Brown and J. E. Brewer (IEEE, New York, 1998), and references therein.
[3] B. Eitan, P. Pavan, I. Bloom, E. Aloni, A. Frommer, and D. Finzi, IEEE Electron Device Lett. **21**, 543 (2000).
[4] P. C. Y. Chen, IEEE Trans. Electron Devices **ED-24**, 584 (1977).
[5] E. Suzuki, H. Hiraishi, K. Ishii, and Y. Hayashi, IEEE Trans. Electron Devices **ED-30**, 122 (1983).
[6] M. H. White and J. R. Cricchi, IEEE Trans. Electron Devices **ED-19**, 1280 (1972).
[7] X. Zhang and G. M. Sessler, Appl. Phys. Lett. **78**, 2757 (2001).
[8] M. Naich, G. Rosenman, and Ya. Roizin, Thin Solid Films **471**, 166 (2005).

[9]E. Suzuki, Y. Hayashi, K. Ishii, and T. Tsuchiya, Appl. Phys. Lett. **42**, 608 (1983).
[10]E. Suzuki and Y. Hayashi, IEEE Trans. Electron Devices **ED-33**, 214 (1986).
[11]A. P. Aganin, V. M. Maslovskii, and A. P. Nagin, Mikroelektronika (Sov.) **17**, 348 (1988).
[12]Z. A. Weinberg, K. J. Stein, T. N. Nguyen, and J. Y. Sun, Appl. Phys. Lett. **57**, 1248 (1990).
[13]Y. C. Park, W. B. Jackson, N. M. Johnson, and S. B. Hagstrom, J. Appl. Phys. **68**, 5212 (1990).
[14]F. Martin and X. Aymerich, Thin Solid Films **221**, 147 (1992).
[15]V. A. Gritsenko, I. P. Petrenko, S. N. Svitasheva, and H. Wong, Appl. Phys. Lett. **72**, 462 (1998).
[16]V. A. Gritsenko, S. N. Svitasheva, I. P. Petrenko, Yu. N. Novikov, Yu. N. Morokov, H. Wong, R. W. M. Kwok, and R. W. M. Chan, Microelectron. Reliab. **38**, 745 (1998).
[17]V. A. Gritsenko, H. Wong, J. B. Xu, R. M. Kwok, I. P. Petrenko, A. B. Zaitsev, Yu. N. Morokov, and Yu. N. Novikov, J. Appl. Phys. **86**, 3234 (1999).
[18]Y. Ma, T. Yasuda, and G. Lucovsky, J. Vac. Sci. Technol. B **11**, 1533 (1993).
[19]J. H. Kim and J. B. Choi, Solid-State Electron. **49**, 795 (2005).
[20]Y. Yang and M. H. White, Solid-State Electron. **44**, 949 (2000).
[21]E. Lusky, Y. Shacham-Diamand, A. Shappir, I. Bloom, and B. Eitan, Appl. Phys. Lett. **85**, 669 (2004).
[22]B. E. Deal, IEEE Trans. Electron Devices **ED-27**, 606 (1980).
[23]C. J. Kang, G. H. Buh, S. Lee, C. K. Kim, K. M. Mang, C. Im, and Y. Kuk, Appl. Phys. Lett. **74**, 1815 (1999).
[24]G. H. Buh, H. J. Chung, and Y. Kuk, Appl. Phys. Lett. **79**, 2010 (2001).
[25]R. E. Paulsen, R. R. Siergiej, M. L. French, and M. H. White, IEEE Electron Device Lett. **13**, 627 (1992).
[26]S.-D. Tzeng, C.-L. Wu, Y.-C. You, T. T. Chen, S. Gwo, and H. Tokumoto, Appl. Phys. Lett. **81**, 5042 (2002).
[27]F. S.-S. Chien, J.-W. Chang, S.-W. Lin, Y.-C. Chou, T. T. Chen, S. Gwo, T.-S. Chao, and W.-F. Hsieh, Appl. Phys. Lett. **76**, 360 (2000).
[28]D. Sarid, *Scanning Force Microscopy: with Applications to Electric, Magnetic and Atomic Forces*, revised ed. (Oxford University Press, New York, 1994).
[29]S. Hudlet, M. S. Jean, B. Roulet, J. Berger, and C. Guthmann, J. Appl. Phys. **77**, 3308 (1995).
[30]G. Lubarsky, R. Shikler, N. Ashkenasy, and Y. Rosenwaks, J. Vac. Sci. Technol. B **20**, 1914 (2002).
[31]S. M. Sze, *Physics of Semiconductor Devices*, 2nd ed. (Wiley Interscience, New York, 1981).
[32]W. Shockley and W. T. Read, Phys. Rev. **87**, 835 (1952).
[33]R. N. Hall, Phys. Rev. **87**, 387 (1952).
[34]H. Aozasa, I. Fujiwara, A. Nakamura, and Y. Komatsu, Jpn. J. Appl. Phys., Part 1 **38**, 1441 (1999).
[35]H. Tanaka, Appl. Surf. Sci. **147**, 222 (1999).
[36]A. Schenk and G. Heiser, J. Appl. Phys. **81**, 7900 (1997).
[37]A. Haque and K. Alam, Appl. Phys. Lett. **81**, 667 (2002).
[38]P. J. McWhorter, S. L. Miller, and T. A. Dellin, J. Appl. Phys. **68**, 1902 (1990).
[39]T. H. Kim, J. S. Sim, J. D. Lee, H. C. Shin, and B.-G. Park, Appl. Phys. Lett. **85**, 660 (2004).
[40]M. Naich, G. Rosenman, Ya. Roizin, and M. Molotskii, Solid-State Electron. **48**, 477 (2004).
[41]V. A. Gritsenko, E. E. Meerson, and Yu. N. Morokov, Phys. Rev. B **57**, R2081 (1998).
[42]V. A. Gritsenko, in *Silicon Nitride in Electronics*, edited by A. V. Rzhanov (Elsevier, New York, 1988), Chap. 6, and references therein.
[43]N. F. Mott and E. A. Davis, *Electron Processes in Non-Crystalline Materials* (Clarendon, Oxford, 1979).
[44]V. A. Gritsenko, E. E. Meerson, I. V. Travkov, and V. Yu. Goltvyanskii, Mikroelektronika (Sov.) **16**, 42 (1987).
[45]F. L. Hampton and J. R. Cricchi, Appl. Phys. Lett. **35**, 802 (1979).
[46]E. Suzuki and Y. Hayashi, J. Appl. Phys. **53**, 8880 (1982).
[47]F. Martin and X. Aymerich, Microelectron. J. **22**, 5 (1991).